Int J Earth Sci (Geol Rundsch) (2017) 106:2527–2547
DOI 10.1007/s00531-017-1445-1

ORIGINAL PAPER

Extension-related buttress-like folds, the western side of the Gulf of Suez rift, Egypt

A. S. A. A. Abu Sharib[1] · M. M. Abdel-Fattah[1] · Y. F. Salama[1] · G. I. Abdel-Gawad[1]

Received: 10 June 2016 / Accepted: 11 January 2017 / Published online: 28 February 2017

Abstract The wedge-shaped St. Paul block, western side of the Gulf of Suez rift, exposes Late Cretaceous beds that are folded into transverse folds. The block is bounded from the east and west by east- and southeast-dipping rift-related normal faults, respectively. This study reveals that the transverse folds are extension-related, and formed due to the buttress-like effect that was created during the movement along the rift-related normal faults. The more competent Eocene hanging-wall block of the N–S-striking fault buttressed against the moving less competent Cretaceous hanging-wall block of the NE–SW-striking fault. A localized zone of shortening developed between the two fault trends causing the intervening wedge-shaped block to be crumpled and folded into a series of kilometer-scale, gentle SSE-plunging folds. The buttressing, within block internal localized strain caused by the zigzag geometry of the NE–SW-striking fault, and the effect of the minor cross fault explain the SSE-to-ESE plunges of the mesoscopic folds. This study turns the attention to the buttress-like effect as one of the mechanisms of extension-related folds during rifting.

Keywords St. Paul block · Extension · Normal fault · Localized shortening · Buttress folds · Gulf of Suez rift

✉ A. S. A. A. Abu Sharib
aabusharib@yahoo.com

[1] Geology Department, Beni-Suef University, Beni-Suef 62511, Egypt

Introduction

Despite the fact that folds are generally compression-related structures that develop during orogenic movements (Abu Sharib and Bell 2011; Abu Sharib 2012, 2015), non-orogenic folds also commonly occur in extensional settings (e.g., Schilsche 1992, 1995; Gawthorpe et al. 1997; Janecke et al. 1998; Gupta et al. 1999; Maurin and Niviere 1999; Corfield and Sharp 2000; Sharp et al. 2000). Extension-related folds include differential compaction-related folds, longitudinal, and transverse folds (Janecke et al. 1998; Schilsche 1995). The latter two categories differ markedly in their axial planes orientations in relation to the associated faults. Longitudinal folds have hinge lines oriented parallel to sub-parallel to the strike of the associated faults, and are represented by drag folds (Fig. 1a), reverse drag folds (Barnet et al. 1987; Mukherjee and Koyi 2009; Mukherjee 2011, 2014) (Fig. 1b), roll-over anticlines (Fig. 1c), and fault-propagation folds (Corfield and Sharp 2000; Sharp et al. 2000) (Fig. 1d). They are attributed to (1) frictional drag along the fault surface (Twiss and Moores 2007; Davis et al. 2012) (Fig. 1a, b), (2) flexuring at the tip of upward propagating faults (Fig. 1d), (3) decreasing fault displacement perpendicular to the strike of the fault (Fig. 1a, b, c), and (4) overlapping fault systems (Fig. 1e–g). Transverse folds, on the other hand, have hinge lines at high angle (perpendicular) to the associated faults, and are attributed to along-strike variations in fault displacement (Fig. 1h).

The Tertiary Gulf of Suez (GOS) continental rift remains a prime focus for studies to understand geometry, types, and mechanism of formation of extension-related folding (Coffield and Schamel 1989; Gawthorpe et al. 1997; Gupta et al. 1999; Sharp et al. 2000; Misra and Mukherjee 2015). The extension-related folds (hanging-wall side) were generally attributed to various

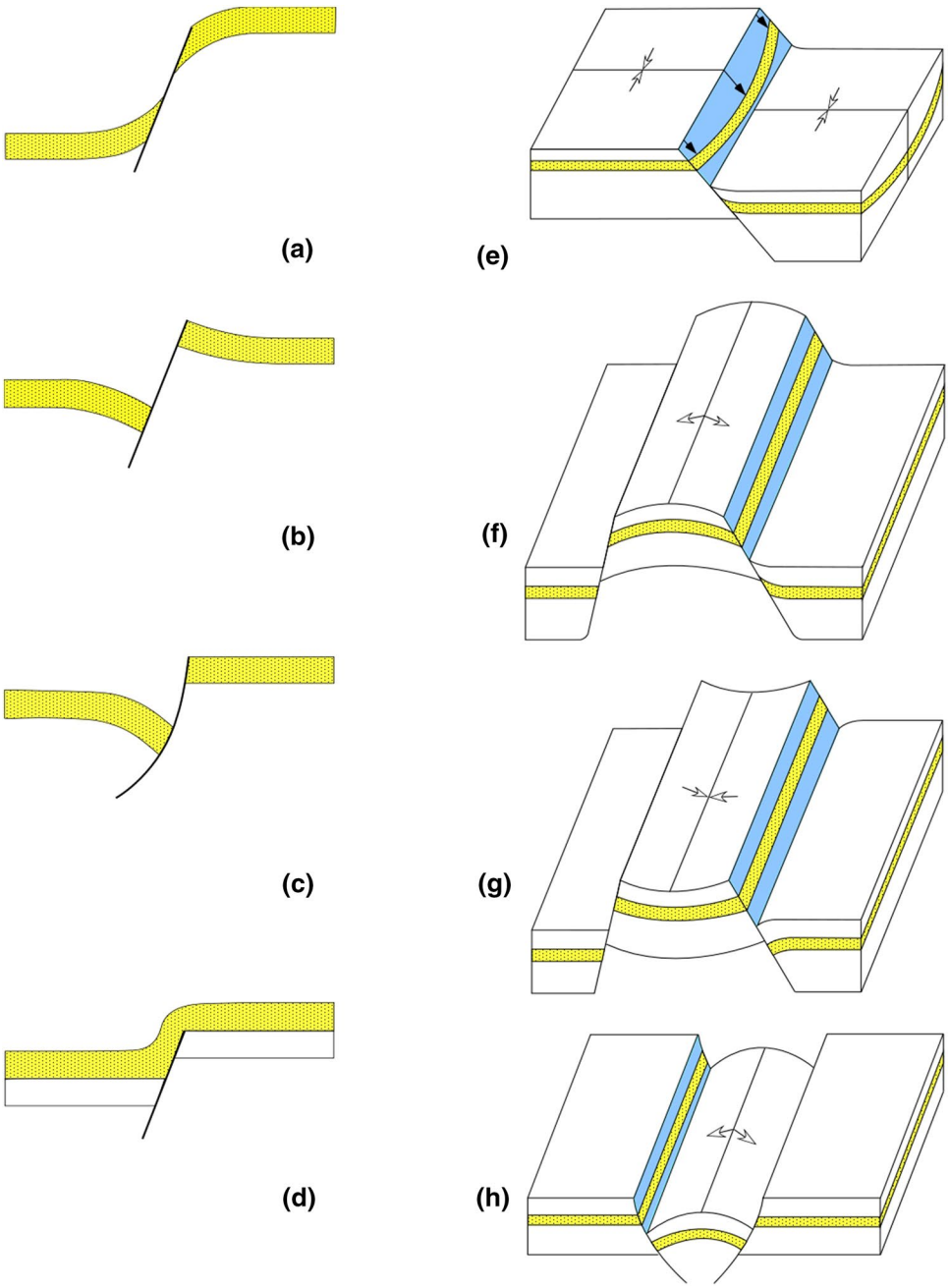

Fig. 1 Cross-sectional views (**a**–**d**) and block diagrams (**e**–**h**) showing fault-related longitudinal and transverse folds. **a** Drag fold. **b** Reverse drag fold. **c** Roll-over anticline. **d** Forced fold. **e** Transverse syncline developed due to along-strike variation of the fault displacement. **f, g, h** Longitudinal anticline (**f, h**) and syncline (**g**) developed in the zones between two completely overlapping planar (**f, g**) and listric (**h**) faults

reasons. Coffield and Schamel (1989) attributed these folds to gentle rollovers above oblique ramps, and to passive draping of poorly consolidated sediments above normal faults. According to Younes and McClay (2002), extension-related folds formed due to the local shortening that developed at the intersection of rift-related normal faults and basement-related shear zones. Growth folding and monoclines above steep blind normal faults during rifting were also proposed (Patton 1982; Moustafa 1987; Moustafa and El-Raey 1993; Gawthorpe et al. 1997; Sharp et al. 2000; Gupta et al. 1999; Misra and Mukherjee 2015). Extension-related folds in the western side of the Gulf of Suez rift received lesser attention.

Detailed lithological/structural mapping showed that Kilometer-scale extension-related close folds are exposed in the St. Paul area, western side of the Gulf of Suez rift, where pre-rift Late Cretaceous ammonite-bearing rocks are folded into a series of SSE-plunging meso-to-macroscopic folds.

This work aims to: (1) determine the nature of the St. Paul folds; (2) introduce a new extension-related folding mechanism (buttressing); and (3) introduce a probable

explanation of the origin of folding of the pre-rift Late Cretaceous rocks in the St. Paul area during the crustal extension that accompanied the Gulf of Suez rifting.

Geologic setting

The Gulf of Suez is (GOS) a ~300 km long, northwest-trending continental rift that separates the Sinai microplate to the northeast from the African plate to the southwest (Fig. 2). Extension along the rift developed as a result of northeastward motion of the Arabian plate relative to the African plate (Fig. 2) during Late Oligocene-Early Miocene (Patton et al. 1994; Purser and Bosence 1998; Bosworth and McClay 2001). However, Sehim et al. (1999) argued, based on the litho- and bio-facies of the oldest syn-rift sediments, that the rifting initiated during the Late Eocene to Early Miocene.

Based on the along-strike abrupt changes in the dip polarity of the rift border faults and intra-rift faults, the GOS rift is divided into three dip provinces (northern, southern, and central), separated by up to 20 km wide Zaafarana-and Morgan- accommodation zones (Bosworth and McClay 2001; Moustafa 2002; Younes and McClay

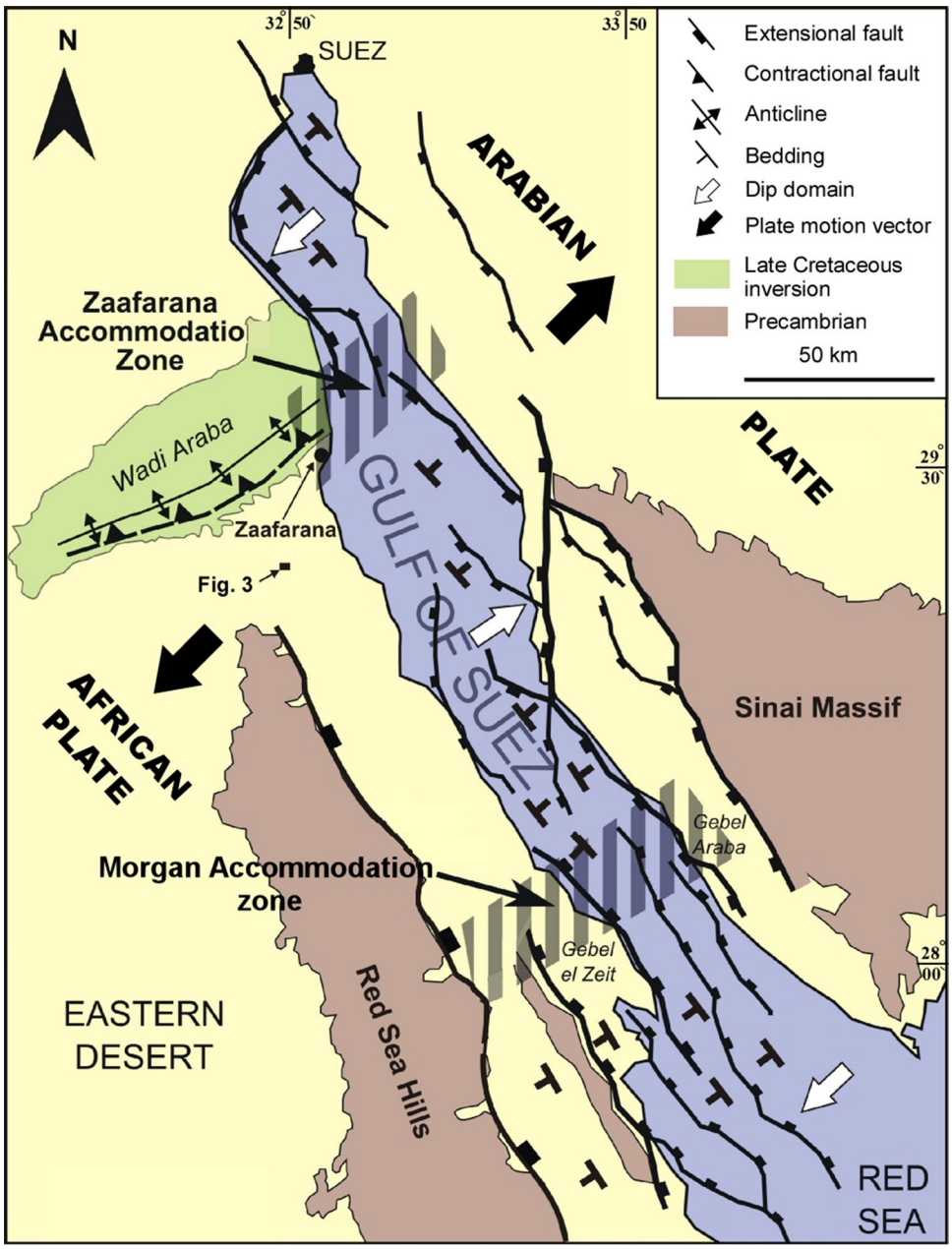

Fig. 2 General structural overview of the Gulf of Suez rift that shows the dip polarity of the rift-bounding and master faults in the three dip provinces, and the two major accommodation zones (*modified after Khalil, 1998;* Bosworth and McClay 2001)

2002) (Fig. 2). The northern- and southern-dip provinces are characterized by NE-dipping master faults (rift border) and SW-dipping beds, while the central dip province is dominated by NE-dipping beds and SW-dipping master faults. The rift-bounding faults are generally listric with the intra-rift faults featuring a classical half-graben style (Patton et al. 1994; McClay et al. 1998).

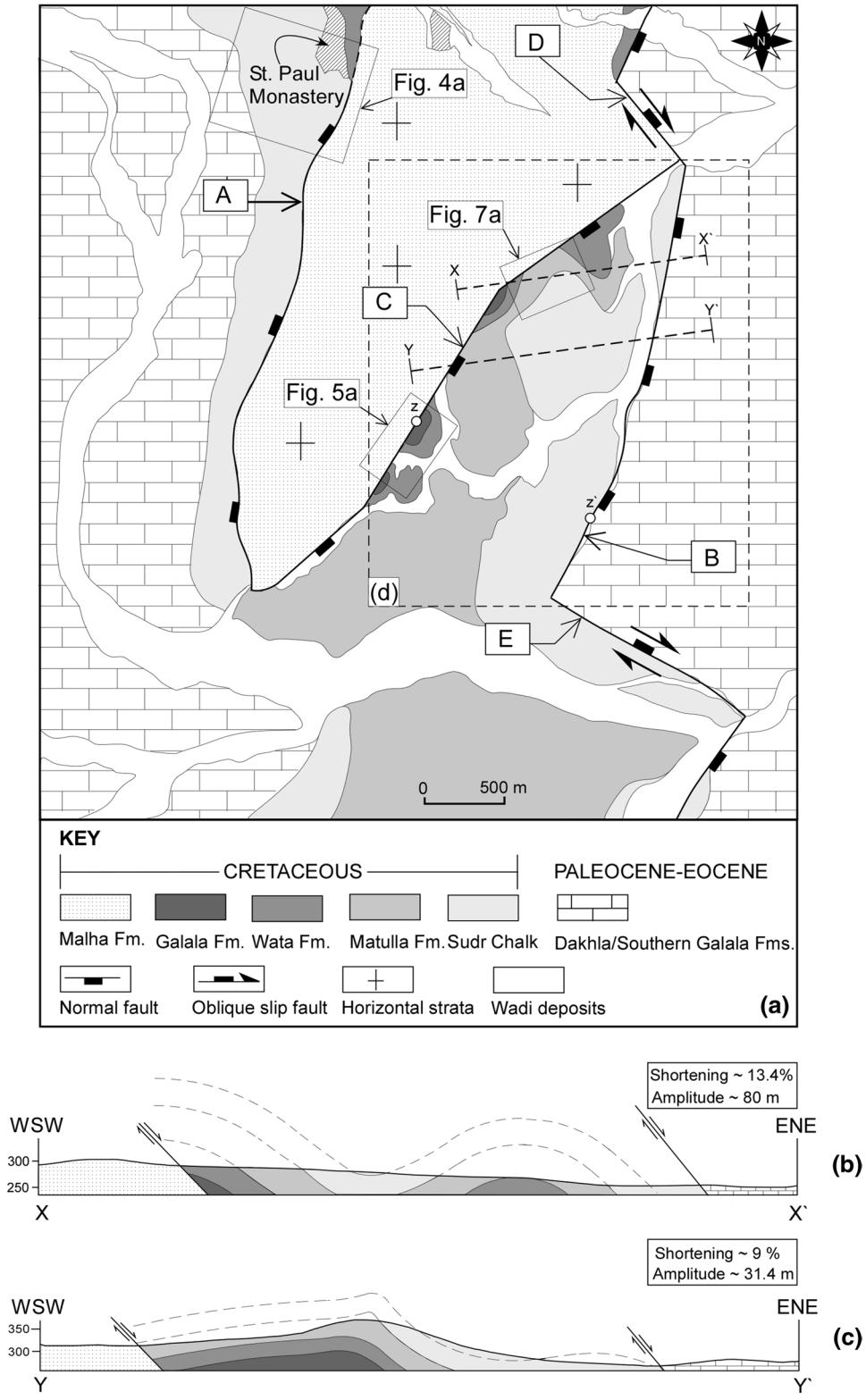

Fig. 3 **a** Geological map of St. Paul area showing the distribution of the exposed rock units and the major faults. **b, c** Structural cross sections along lines X–X′ and Y–Y′, respectively. **d** Detailed structural map [*inset* labeled (**d**)] showing the NE–SE and N–S-striking faults and the major NW-SSE-oriented folds. **e** Lower hemisphere projection of the pole to bedding planes. **f** Lower hemisphere projection of the axes of mesoscopic folds and folded ammonites

Fig. 3 (continued)

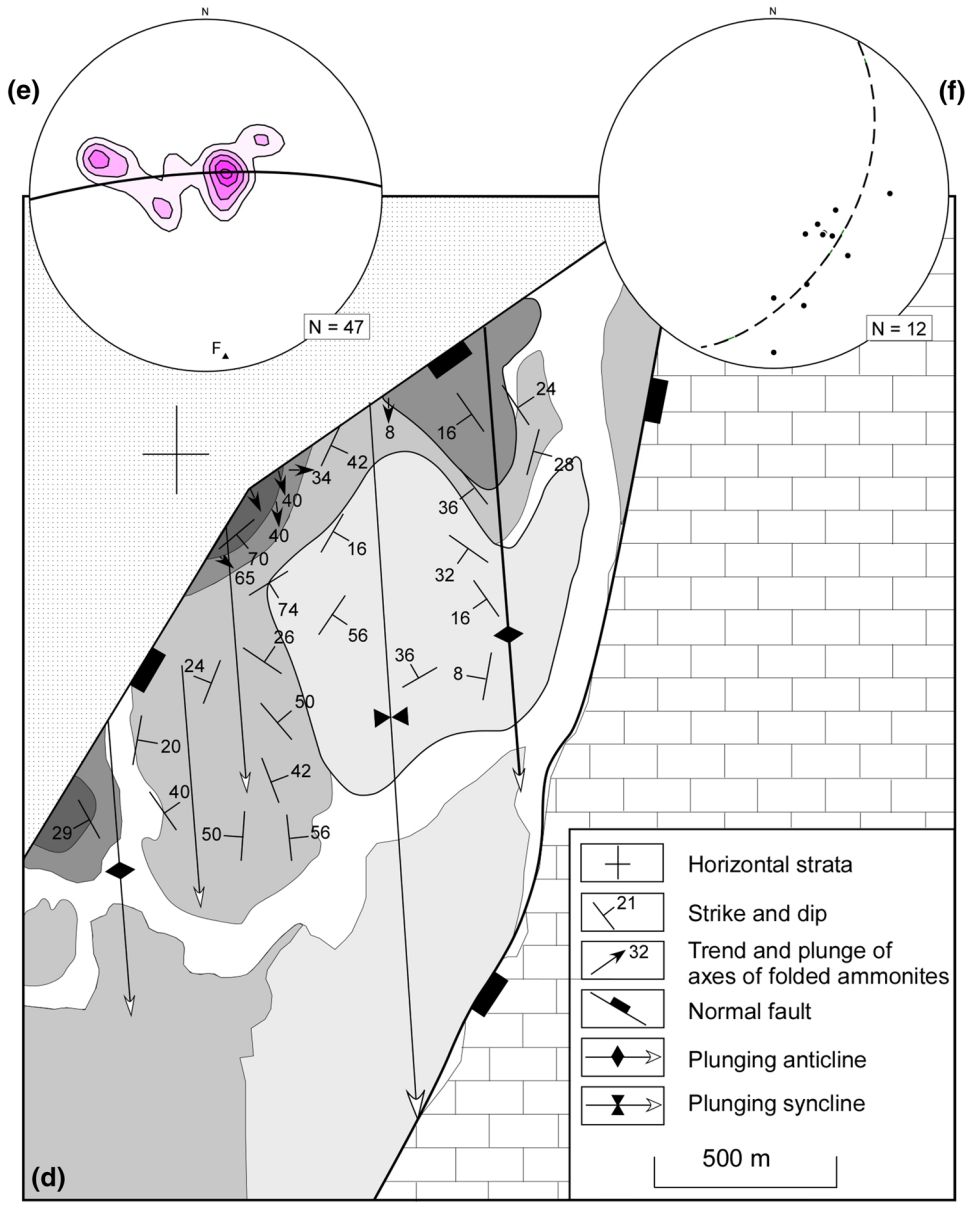

The St. Paul Monastery area, Southern Galala, Egypt, lies 30 km southwest of Zaafarana city, and is located in the central dip province on the western side of the Gulf of Suez rift (Figs. 2, 3). It is dissected by a group of variably trending rift-related normal faults as well as oblique slip faults. The St. Paul area exposes a pre-rift conformable succession of alternating Early-to-Late-Cretaceous siliciclastic- and carbonate facies, overlain unconformably by a predominantly Paleocene–Eocene carbonates facies. Different formation names have been assigned to the Cretaceous and lower Tertiary succession exposed in the St. Paul area (Awad and Abdallah 1966; Abu Khadrah et al. 1987; Kuss et al. 2000; Scheibner et al. 2001; Abdel-Gawad et al. 2007; Höntzsch et al. 2011). These formations are arranged from bottom to top as: Malha, Galala, Wata, Matulla, Sudr, Dakhla, Southern Galala and Thebes (Fig. 4a, b). The Malha Formation consists mainly of fluvial sandstone of Aptian-Albian age (Cretaceous) (Abdallah and El Adindani 1963). The Galala Formation is composed of about 51-m-thick succession of alternating sandstone and shale with rare intercalations of dolostone or marl of Late Cenomanian age (Cretaceous). The Late Cenomanian fauna include *Ceratostreon flabellatum, Rhynchostreon suborbiculatum, Ilymatogyra africana, Costagyra olisiponensis, Eoradiolites liratus, Thomelites sornayi*, and *Hemiaster cubicus*. The upper part of the formation occupies the uppermost Cenomanian ammonites *Vascoceras cauvini* and *Rubroceras alatum*. The 61-m-thick Wata Formation is of

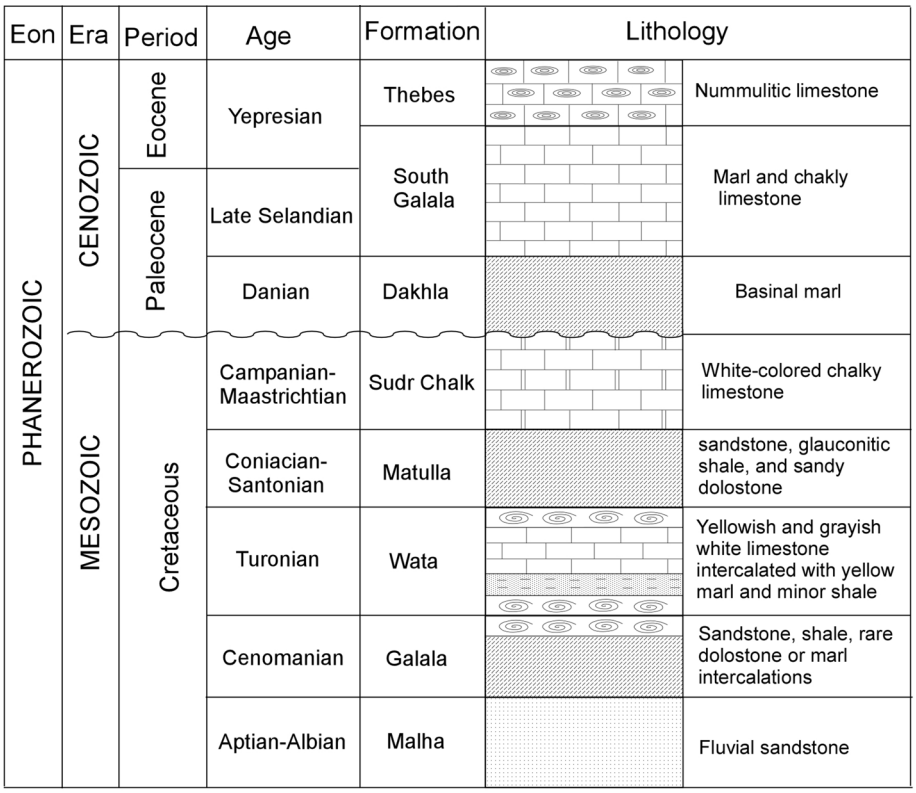

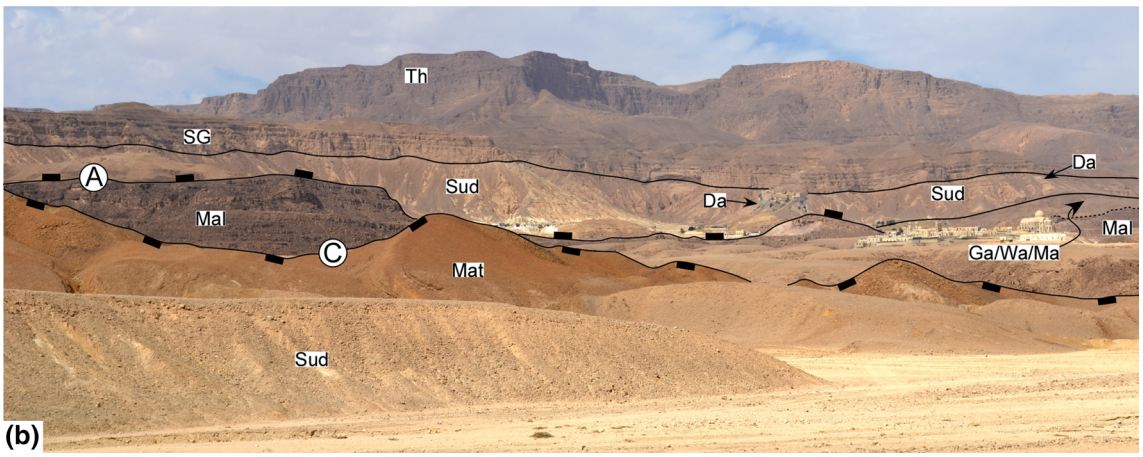

Fig. 4 **a** Stratigraphic section of the rock units exposed in the St. Paul area with the most common ammonite species present. **b** Panoramic view shows the different formations exposed in the St. Paul area: Sudr chalk (Sud); Matulla (Ma); Wata (Wa); Malha (Mal); Galala (Ga); Dakhla/Southern Galala (Da/SG)

Turonian age, and is composed of yellowish- and grayish-white limestone interbedded with yellow marl and minor shale. The Turonian ammonites recorded at the base and top of the formation are *Choffaticeras segne, Choffaticeras securiforme, Thomasites rollandi*, and *Coilopoceras requienianum*. The Matulla Formation is made up of about 150-m-thick interbedded sandstone, glauconitic shale, and sandy dolostone of Coniacian–Santonian age. The Sudr Chalk is composed of about 100 m thick white-colored chalky limestone of Campanian–Maastrichtian age (Awad and Abdallah 1966; Abdel-Gawad et al. 2007). The Paleocene and Early Eocene marl and limestone ramp succession is represented by two formations: the Dakhla at the base; the Southern Galala at the top (Kuss et al. 2000; Galal and Kamel 2007). The Dakhla Formation is made up dominantly of basinal marls of Danian age (Kuss et al. 2000).

The Southern Galala Formation is made up of a succession of marl and chalky limestone of Late Selandian-Early Yepresian age. It is topped by the Early Eocene (Yepresian) nummulitic limestone of the Thebes Formation.

Structural elements in the St. Paul area

Faults

Normal faults

Normal faults, which are the most abundant type of faults, occur in two main rift-related trends: N–S (N015°) and NE–SW (N030°) (Jarrige et al. 1986). The N–S-trending faults are represented by west- and east-dipping faults (A and B, respectively) forming a horst structure (Fig. 3). The fault B, which extends for about 5 km and continues north-and-southwards outside the study area, juxtaposes the Eocene block (eastern side of the map) against the Cretaceous block. The latter is faulted against the high relief Eocene-Late Cretaceous block (western side of the map) along the fault A (Fig. 3). The fault A cuts across the area for about 3.5 km until it ends against fault C (Fig. 3). The sub-horizontal strata (~3–5°) in the footwall block of fault A reveals that this fault is a rift shoulder fault.

The fault C is segmented into three segments: a northern and a southern NE–SW striking; and a central NNE–SSW-striking. It extends for about 3 km connecting obliquely faults A and B. It juxtaposes the sub-horizontal beds of the Early Cretaceous Malha Formation against the moderately to steeply-dipping Late Cretaceous succession (Figs. 3, 5a). It is a steep (~60°) SE-dipping fault with a gradual decrease of the fault plane inclination towards the SE. The strata close to the fault are steeply-dipping (~60°) with a decrease in the amount of dip (~30–40°) due southeast. Proper

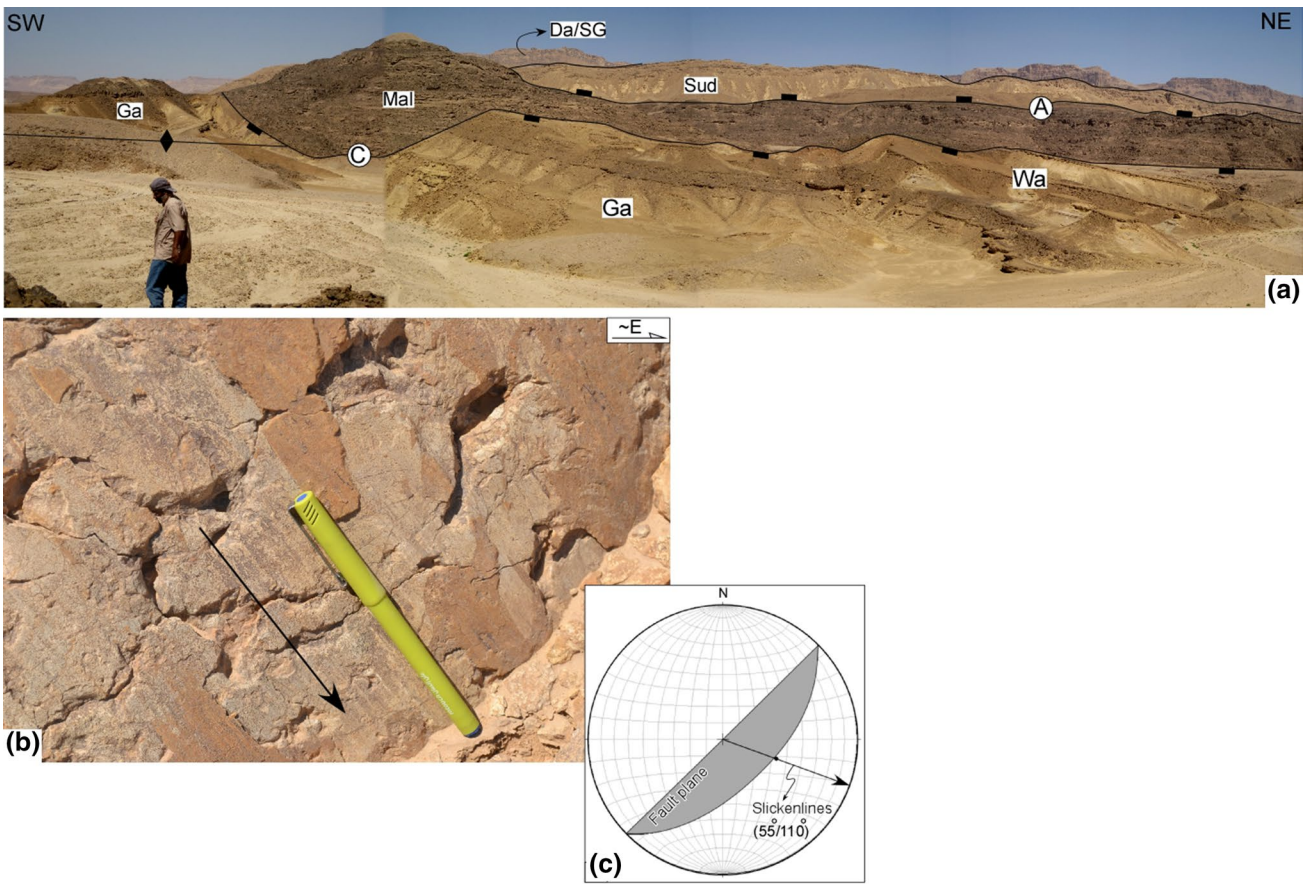

Fig. 5 **a** Panoramic view, at a high angle to the trend of the fold axis, showing the major non-plunging anticline developed in the hanging-wall block of the NE–SW-striking fault C that juxtaposes the Early Cretaceous Malha Formation (Mal) against the Late Cretaceous succession. The N–S-striking fault A that juxtaposes the Sudr Chalk against the Malha Formation appears in the background. Note the high angle between the strike of the fault and the trend of the fold hinge. **b** Steeply-dipping slicken lines that plunge at 55° towards 110° indicating a down-dip movement

dip slip movement on the fault is evidenced by steep, SE (down-dip)-plunging slickenlines (Fig. 5b), some of which are well-developed on some Turonian ammonites. Differential along-strike displacement of fault C is evidenced by the northeastward decrease in the thickness of the Malha Formation in the footwall block of the fault.

Strike slip and transfer faults

Strike slip faults are subsidiary and have generally small horizontal displacements. These displacements are clearly evidenced by horizontal slickenlines which are preserved on some minor fault planes. However, field observation shows that some fault planes record a rather complex displacement history, consisting of overprinting translational and rotational movements (Fig. 6). Fault B is segmented into three synthetically-approached segments (e.g. Morley et al. 1990) that are linked through two transfer faults (D and E) that extend for about ~750 to ~1500 m in NNW–SSE-to-NW–SE directions, respectively (Fig. 3). The right-lateral sense of movement of these faults is basically documented through the offset of the lithological boundaries (Fig. 3).

Folds

The Late Cretaceous rocks are mesoscopically- to macroscopically folded. The folds are restricted to the hanging wall of the zigzag-shaped fault C (Fig. 3), and extend >2 km (Fig. 3) in the study area and continue outside it for a considerable distance. No folds were detected in the hanging-wall blocks of the N–S-striking faults (A and B), where the bedding is primarily sub-horizontal.

Macroscopic folds

The macroscopic folds are represented by two asymmetrical upright anticlines separated by a syncline with gentle SSE-plunging axes and interlimb angle of 70–120° (Fig. 3d, e). The southern and northern anticlines are cored by the Cenomanian Galala Formation overlain by the Wata and Matulla formations (Figs. 3, 5a). The syncline is cored by the very thick Sudr chalk (Figs. 3, 7).

Mesoscopic folds

The mesoscopic folds are represented by locally folded ammonites in the Wata and Galala formations (Fig. 8), and rare kinks developed in the oyster-bearing, shale-dominated Matulla Formation. The folds have moderate to steep, SSE–ESE-plunging axes (Fig. 3f). The folded ammonites are restricted to a very narrow zone, where the steeply-dipping Galala and Wata formations meet fault C towards its southwestern end (Fig. 3).

Discussion

The relative timing of the normal faults: the N–S vs. NE–SW trends

The geometry of the rifts is strongly controlled by the pre-rift fabrics (e.g., East African rift, McConell 1972;

Fig. 6 Complex movement along a minor cross fault cutting through the Matulla Formation

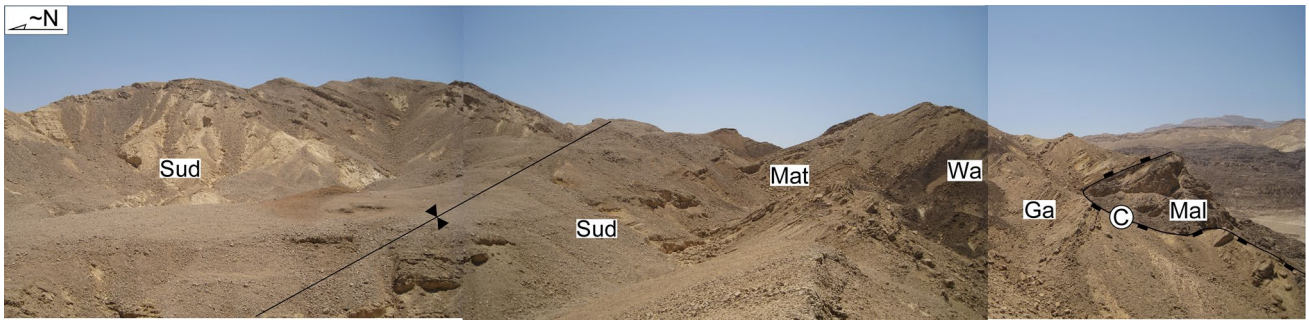

Fig. 7 Panoramic view showing the major SSE-plunging syncline in the St. Paul area: Sudr chalk (Sud); Matulla (Ma); Wata (Wa); Malha (Mal); Galala (Ga)

Kazmin 1979; the Baikal rift; Florensov 1966; the Oslo rift; Bederke 1966; the Rio Grande rift; Faulds et al. 1990; Beck and Chapin 1994; the Suez rift, Jarrige et al. 1986; Younes and McClay 1998, 2002). Four main fault trends are recorded in the GOS: the NW–SE (Clysmic), N–S to NNE–SSW (Aqaba), E–W to WNW–ESE (Duwai), and NE–SW (Cross) trends. These trends represent inherited Pan-African basement fabrics (fractures, faults, and shear zones) that reactivated during the Neogene extension. The typical zigzag geometry of the GOS is attributed to the link between the N–S and NW–SE trends (e.g., Lyberis 1988; Jarrige et al. 1986; Younes and McClay 2002). Relative age relationships show that the pervasive NE–SW-trending faults displace and cross cut the N–S trend (Younes and McClay 2002). The former trend is widespread in Sinai Peninsula, in the sedimentary cover in the Gebel Dara and Wadi Araba areas (Jarrige et al. 1986, 1990), and in the basement rocks on both margins of the Suez rift. Relatively younger NE–SW-trending normal faults are well-documented throughout the Gulf of Suez rift (Vargo et al. 1993; Sehim et al. 1999). Sub-surface data of the offshore Warda field, about 50 km northwest of the study area, show the N–S-striking normal faults that are displaced by the NE–SW-striking ones (Vargo et al. 1993; Fig. 4 of Younes and McClay 2002).

In the St. Paul area, the NE–SW-striking normal fault C abuts against the N–S-striking normal fault B with a fault displacement decreasing to minimal values, where both faults meet (Fig. 3). The latter observation is evidenced by the differential uplift of the Malha Formation along the footwall block of fault C. The fault C shows a relatively younger extensional event than faults A and B. This conclusion is mainly derived from the horizontal attitude of the strata in the hanging walls of faults A and B and the footwall of fault C. Moreover, this conclusion is furtherly supported by the restriction of the folds to the wedge-shaped block delimited by the faults B and C. However, the fault C does not displace the relatively younger fault B. This could be attributed to the dramatic northeast dissipation in the stresses responsible for the further northeastward propagation of the fault C. This led to a decrease in the magnitude of the fault displacement in the latter direction. Consequently, the fault C became arrested against the fault B.

Furthermore, what we have is two apparently intersecting faults B and C with one of which is relatively younger and cross cuts/displaces the other. Therefore, to determine the relative timing between both faults, we introduce the assumption that the fault B displaces fault C and that both faults do not intersect at the tip point of the latter fault and compare the resultant geometry with our field observations. Therefore, having such assumption, one should expect a more complex faulted blocks in the hanging wall of the fault B (Fig. 9). Accordingly, a wedge-shaped down-faulted Cretaceous block should have been formed between the fault B and the displaced fault C (Fig. 9). Accurate inspection reveals no record of the Cretaceous rocks nor displaced fault C trace in the hanging-wall block of fault B (Fig. 3). This excludes the possibility that the fault B is younger and cuts across fault C.

Summing up, the movement along the fault C can be interpreted by a relatively younger localized NW–SE extension. The latter might have been caused possibly by the compiled effect of the reactivation of the pre-rift N–S-striking structure (now fault B) during the general N60°E Tertiary extension, and the dextral movement along the NW–SE-striking transfer fault E (Fig. 10). However, two orthogonal extension directions (NE–SW and NW–SE) during the Tertiary extension tectonics can also be considered (e.g., Rosendahl 1987; Oesterlen and Blenkinsop 1994).

The relative timing of the folds in relationship to the faults

In discussing the relative timing between the folds and the bounding rift-related fault C, a compelling question arises,

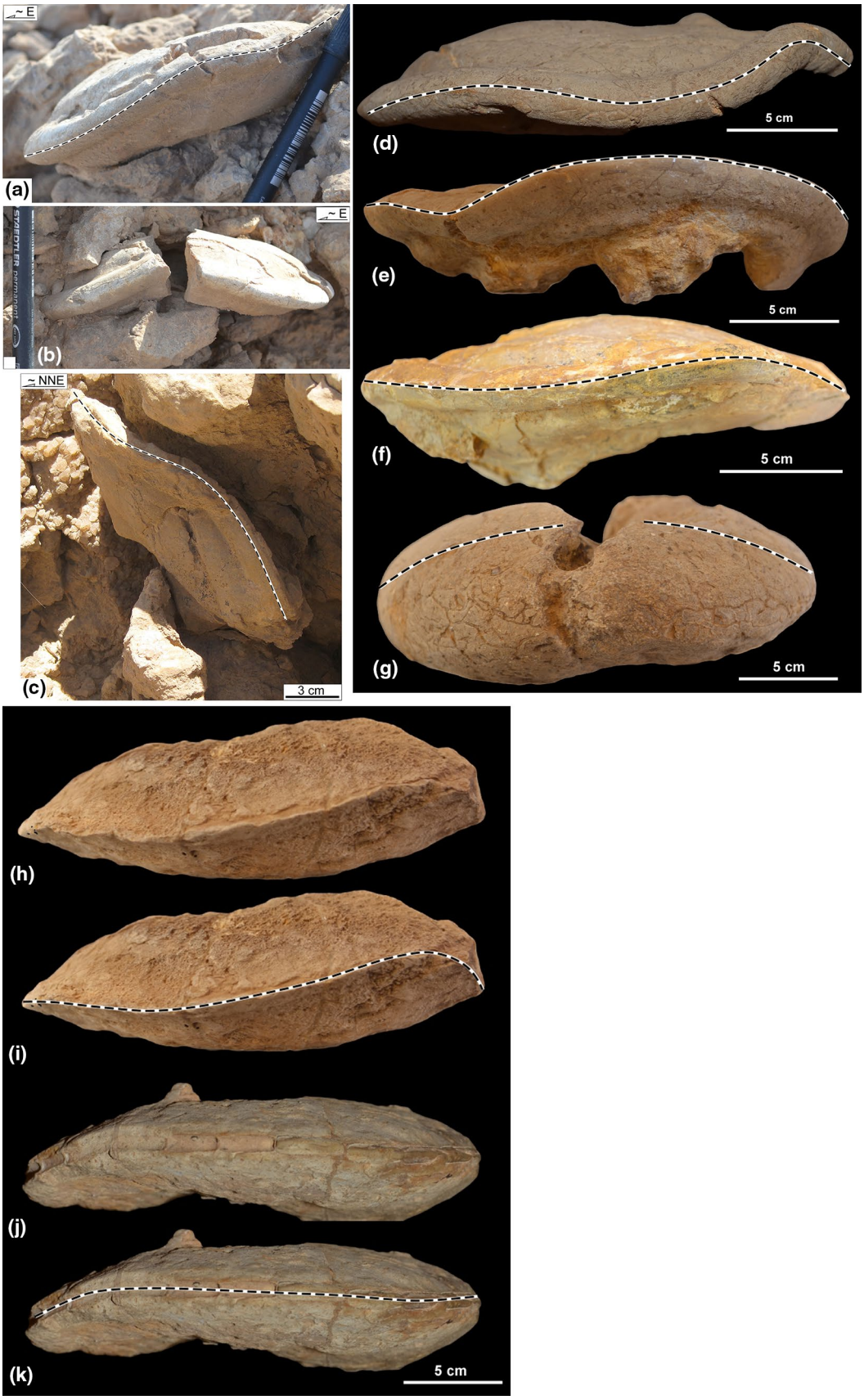
~ E
(a)
~ E
(b)
~ NNE
(c)
3 cm
(d)
5 cm
(e)
5 cm
(f)
5 cm
(g)
5 cm
(h)
(i)
(j)
(k)
5 cm

◂**Fig. 8** **a** Plan view of folded Turonian ammonite, *Choffaticeras securiforme*, in Wata Formation. The fold axis plunges 34° towards 165°. Note the development of extension fractures along the hinge zone. The part of the marker pen is 8 cm long. **b** Plan view of Turonian ammonite, *Choffaticeras securiforme*, Wata Formation, has been completely split along the hinge zone. The fold axis plunges towards 174° at 22°. The part of the marker pen is 7.5 cm long. **c** Plan view of folded Turonian ammonite, *Choffaticeras securiforme*, in the Wata Formation. The fold axis plunges towards 112° at 55°. **d–k** Well-developed folded periphery in some float ammonites: (**d–f**) *Choffaticeras securiforme*, Early Turonian, Wata Formation, **g** *Vascoceras cauvini*, Late Cenomanian, Galala Formation, **h–k** *Choffaticeras segne*, Early Turonian, Wata Formation

are these extension- or compression-related folds? The Late Cretaceous–Early Tertiary time witnessed a major compressional event that recorded the collision between the Afro-Arabian and Eurasian plates. This tectonic event is manifested by a belt of NE–SW-trending Folds (Syrian Arc System) that extends in the North Western Desert and Sinai in Egypt, and continues northeastwards in the Naqb desert and Syria. However, the compression-related folds scenario cannot be true for the St. Paul folds for many reasons. First, the horizontal position of the Lower Cretaceous Malha Formation in the footwall block of fault C excludes the idea of a major folding of the Cretaceous rocks. Second, the assumption that the folds originated as a flat-and-ramp structure accompanied the movement along an originally NW-vergent reverse fault (now fault C) does not explain the en-echelon pattern of the St. Paul folds. In the classical example of the flat-and-ramp geometry during reverse faulting (e.g., Boyer and Elliott 1982), the folds are generally monoclines (sensu-lato), where the affected strata are commonly sub-horizontal on the flat part of the fault, and steepen as they climb the fault ramp. Moreover, the absence of internal reverse/thrust faults in the Late Cretaceous conformable succession in the hanging-wall block of the fault C excludes the idea that the St. Paul periodic folds originated as a series of flat-and-ramp structures accompanied a series of NW-vergent imbricate reverse faults. Furthermore, the zigzag geometry of fault C requires a component of dextral transpression along the oblique ramp, and consequently the development of an array of en-echelon left-stepping, NE–SW-trending folds (Fig. 11). The trend and the sense of stepping of the St. Paul folds are opposite to those formed during the compression-related scenario (Figs. 3, 11), and yet no offset of the lithological boundaries across the fault C has been recorded. Hence, the extension-related folding scenario is the most appropriate for the development of the St. Paul folds.

Transverse vs. longitudinal folds

The gently SSE-plunging folds are spatially associated with fault C, and have their axial planes oriented highly oblique to it. Consequently, these folds are interpreted as transverse- or oblique- folds rather than longitudinal ones. Oblique folds commonly develop between en-echelon segments of oppositely dipping normal faults (e.g., Faulds et al. 2002). Since the two N–S-striking faults A and B completely overlap with a shared horizontally-bedded footwall block, the term oblique folds cannot apply to the St. Paul folds. Consequently, transverse folding is the most appropriate term for the folds. However, in contrast to the typical fault-related transverse folds formed in

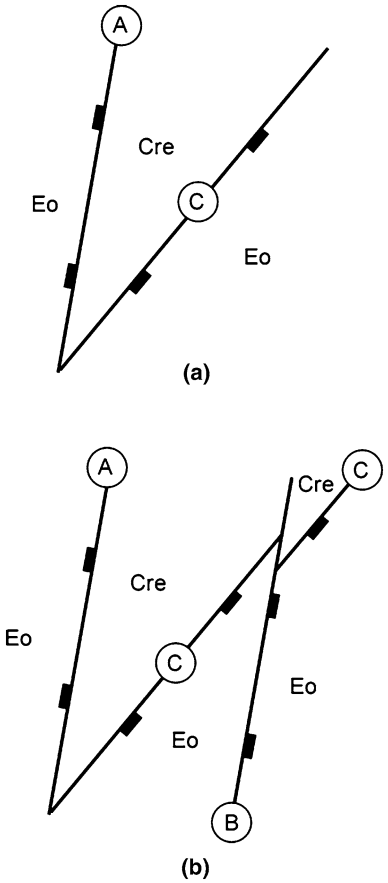

Fig. 9 Two sketches **a** and **b** refutes the idea that the fault B is relatively younger and cuts across the fault C. Assuming that the faults A and B are relatively younger than fault C (**a**) and that the latter fault is crossed by the fault B (**b**) would create complex fault geometries with wedge-shaped Cretaceous block in the hanging wall of fault B. See the text for the explanation. Cre: (Cretaceous); Eo: (Eocene); A, B, and C: (the N–S and NE–SW-striking faults, respectively)

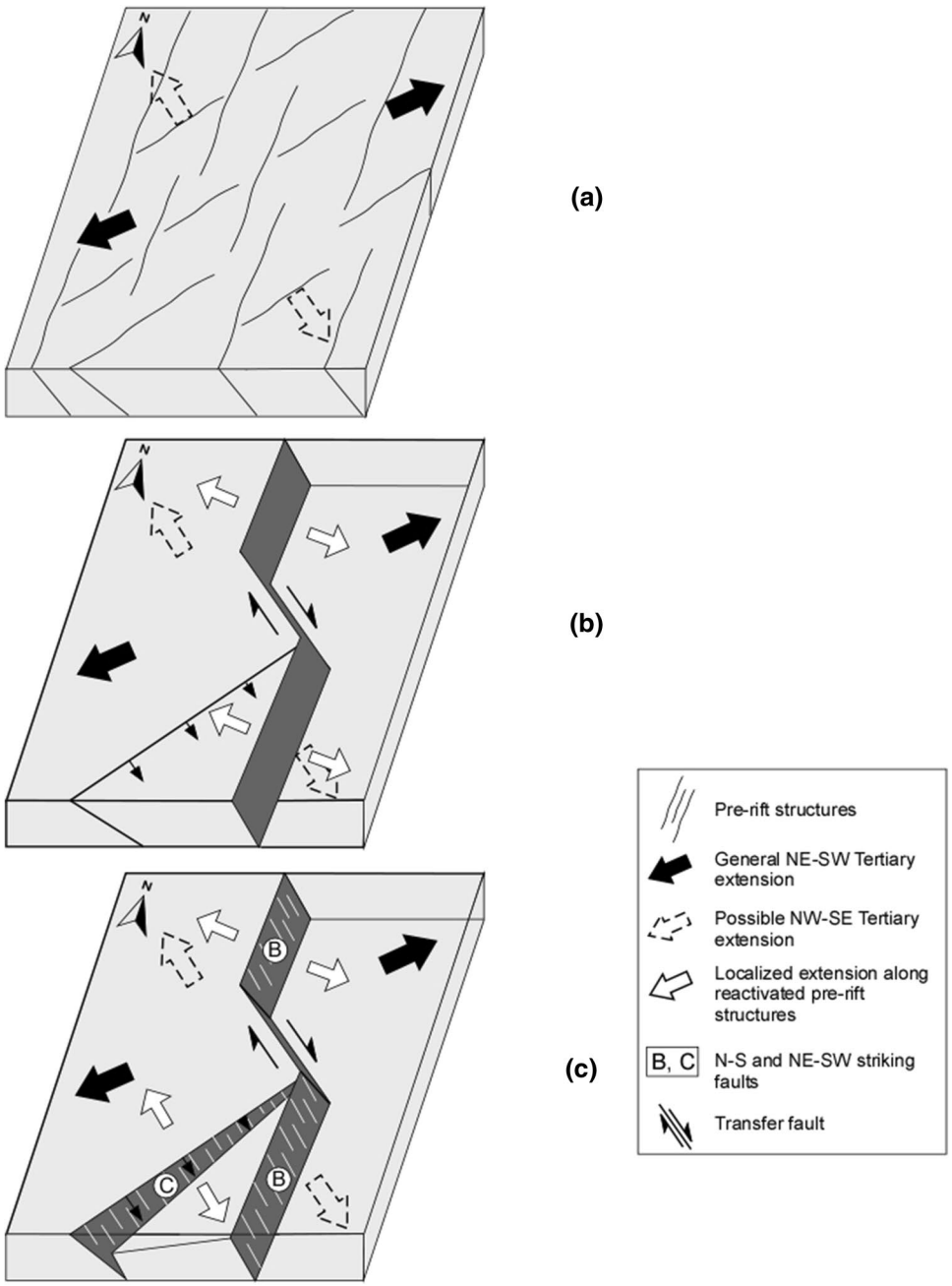

Fig. 10 Schematic model illustrating the possible progressive development of the NE–SW-striking fault C. **a** Pre-rift N–S and NE–SW-striking structures at the NE–SW Tertiary extension. **b** Reactivation of the N–S-striking structures, being the more favourable orientation for extension, into normal faults. **c** Reactivation of the NE–SW-striking structures into relatively younger normal faults through the localized extension created by the interplay between the general NE–SW tertiary extension and the movement along the transfer fault connecting the two segments of the relatively younger N–S-striking faults

an extensional regime with fold hinges oriented at high angles (nearly perpendicular) to the fault plane (e.g., Fig. 1e), the folds in the St. Paul area have acute angles with the bounding fault C.

Some fault planes record a rather complex displacement history, consisting of overprinting translational and rotational movements (Fig. 6). The latter movement along some minor cross faults that are oriented at high angle to the master NE–SW fault might have modified the angular relationship between the transverse folds and the bounding fault.

Extension-related transverse folds

The major rift-related N–S-striking horst structure that developed between the two overlapping normal faults divides the St. Paul area into the undeformed Eocene hanging-wall blocks and the Cretaceous footwall block (Fig. 3). The latter is dissected by the relatively younger NE–SW-striking fault C. The juxtaposition of the macroscopically-folded Late Cretaceous hanging-wall block against the horizontally-bedded Early Cretaceous Malha Formation in the footwall block across the fault C implies

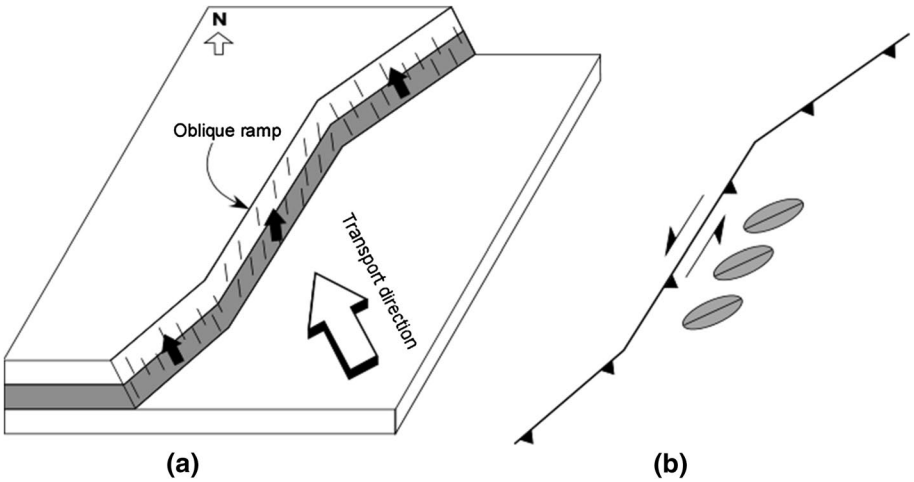

Fig. 11 **a** Schematic diagram illustrates the movement along the fault C during the pre-rift NW–SE-trending compression. **b** Development of an array of en-echelon left-stepping, NE–SW-trending folds (in plan view) as a consequence of a transpressional regime created due to the movement along the oblique ramp of the zigzag-shaped fault C

that the St. Paul transverse folds are extension-related structures that formed contemporaneous with the later rift-related fault.

The origin of the St. Paul folds

The lack of the double plunging geometry of the St. Paul folds precludes their development by along-strike displacement variation of the bounding fault C (for an analog, see Fig. 1e, and Khalil and McClay 2002). Similarly, the lack of the monocline geometry of the folds excludes the idea that the folds originated as forced folds above either a propagating high angle blind normal fault or a sub-surface fault scarp (e.g. Fig. 1d). Moreover, the ~80 m amplitude (Fig. 3b), the kilometer scale, and the obliquity of the folds to the bounding fault C refute the notion that they formed as normal fault-related drag folds (e.g., Fig. 1a, b, c).Furthermore, the horizontal position of the Early Cretaceous Malha Formation in the footwall block of the west-dipping normal fault A (Fig. 3) is a key structural element. It excludes the possibility that the kilometer-scale transverse folds predate the rift-related NE–SW-striking fault and that they were developed originally as an array of en-echelon NW–SE-striking folds that are attributed to the movement along a major pre-rift right-lateral strike slip fault (Fig. 12a). If this was the case, the NE–SW fault would be a later structure across which the hanging and footwalls are folded (Fig. 12b). On the other hand, the fact that fault C separates horizontally-bedded (Malha Formation) and macroscopically-folded domains excludes the idea that the folds originated as longitudinal folds between the two completely overlapping faults A and B (e.g., Fig. 1f, g). The relatively younger NE–SW-striking fault, in this case, would be separating two gently folded domains.

There are no offset of lithological boundaries across or horizontal movement along the entire length of fault C. These observations exclude the possibility that the St. Paul folds formed as an en-echelon array of NW–SE-trending folds as a consequence of movement along an originally left-lateral strike slip fault C that has been reactivated during the Tertiary extension.

Considering the zigzag geometry of the fault C, the movement of the Late Cretaceous hanging-wall block along the fault might have created alternating zones of localized extension and shortening (Fig. 13a). However, applying orthographic projection technique showed that the amount of shortening created by the geometry of the fault is estimated to be only ~3% (Fig. 13b), whereas restoring the folds to the undeformed state in a direction perpendicular to the plunge direction yielded a total shortening of ~13% (Fig. 3b). Similarly, the amounts of shortening (Fig. 13c) estimated from restoring both the rooted and transferred deformed ammonites to the unfolded state range from 1 to 10%. This implies that the zigzag geometry of the fault C might have contributed to the overall shortening of the SE-moving hanging-wall block but was, of course, not the sole mechanism for the folding. Zigzag-fault pattern at the scale of rift-bounding and intra-rift faults is very common and well-documented in the Gulf of Suez rift (Garfunkel and Bartov 1977; Jarrige et al. 1986; Moretti and Chénet 1987; Colletta et al. 1988; Meshref 1990; Moustafa 1993; Patton et al. 1994; Schutz 1994; Bosworth 1995; McClay et al. 1998).

In addition, the horizontal strata in the hanging walls of the faults A and B and the footwall of fault C imply that the strata in the hanging wall of the latter fault were horizontal prior to the faulting. The steeply-dipping (~60°) fault C juxtaposes Early- and Late-Cretaceous

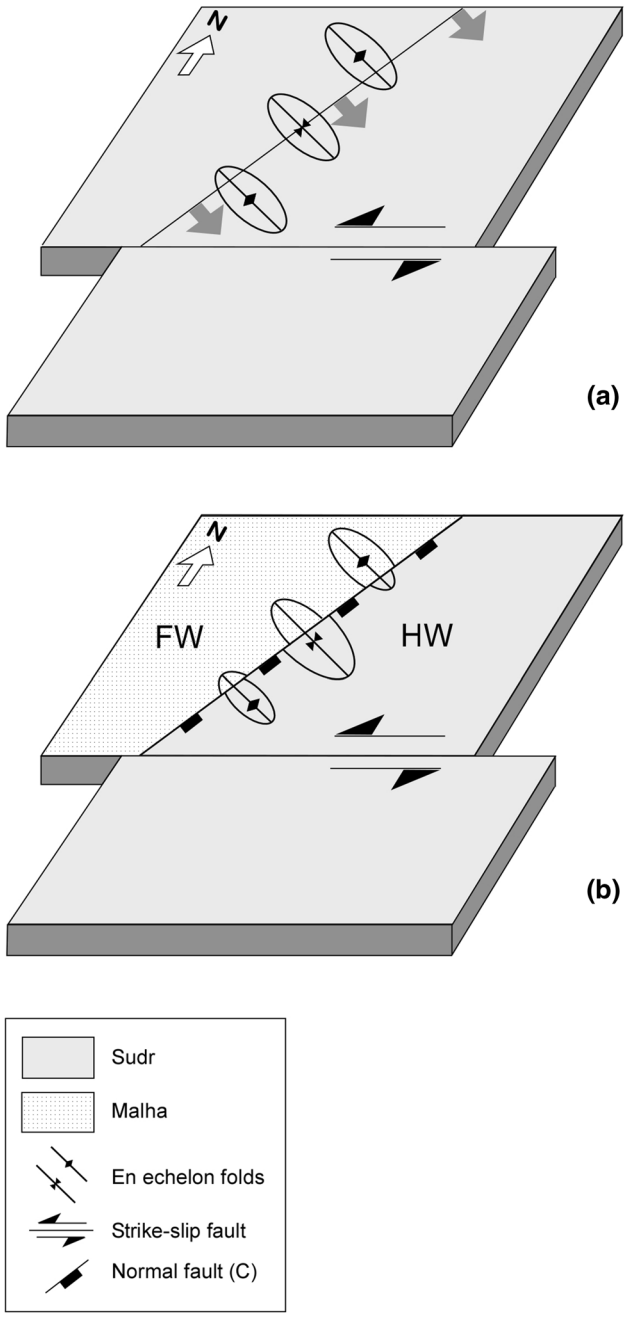

Fig. 12 Schematic model refuting the pre-rift wrenching as an origin of the St. Paul folds. **a** Development of an array of echelon left-stepping, NW–SE-trending folds accompanying a pre-rift left-lateral strike slip fault. **b** Development of a rift-related NE–SW-trending fault C crosscutting the early-formed folds

blocks in the foot- and hanging walls, respectively. Outside the disturbed fault zone, the thicknesses of the Cretaceous strata are well-measured (Fig. 4a). Accordingly, the throw of the fault is roughly estimated to be about 100 m, assuming no drastic along-strike thickness changes of the different formations. Such throw (100 m) requires about 58 m heave that increases as the fault flattens downwards. The maximum, present-day, spacing distance between the faults C and B is 1250 m (distance between points z and z` in Fig. 3), and so restoring the disturbed strata in the hanging wall of fault C into the position prior to faulting would produce a total outcrop distance of about 1310 m. Hence, the movement along the fault C would have shortened the southeast moving less competent Cretaceous hanging-wall block by an amount of, at least, 4.5%. The amount of shortening estimated by restoring the folded hanging-wall strata of fault C into the undeformed state in a direction parallel to the maximum outcrop distance line (z–z′) line in Fig. 3 is about 4% resembling the shortening produced by the movement along fault C (see above). Therefore, we introduce an alternative new folding mechanism, wherein the Late Cretaceous beds in the down-faulted St. Paul block are folded into a series of extension-related transverse buttress-like folds. Well-documented examples show that the buttress folds are reactivation structures form in the hanging wall of the non-planar normal faults during basin inversion (e.g., Dart et al. 1995; McClay et al. 1998; Baum et al. 2008). The movement along the flat segment of the fault is much easier than that along the ramp which acts as a buttress inhibiting the movement and causing shortening and folding of the hanging-wall block (Fig. 14a, b). We adopt another type of buttressing whereby the buttress-like folds develop when the strata are pushed against a stationary or partially stationary wall in a similar way to bulldozer-like effect (Fig. 14c, d). The folds in such a model form due to a combination of buttressing and space accommodation problem (Fig. 14c, d). Surface and sub-surface positive inversion structures are widespread and well-documented during the Late Mesozoic-Paleogene Syrian Arc tectonic event (Moustafa 2013, Fig. 2). Sub-surface examples include the Kattaniya, Mubarak, Alamein-Razzak, and Matruh basin folds in the northern Western Desert (Bakr and Helmy 1990; Nemec 1996; El-Shaarawy et al. 1992; Abd El-Aziz et al. 1998; Moustafa 2008; Moustafa et al. 2002, 2008). Surface outcrops of inverted basins include the Maghara, Halal, and Yelleg folds in northern Sinai, and Wadi Araba Anticline in the northern Eastern Desert (Moustafa and Khalil 1995). The latter is about 30 km north of the study area (Fig. 2). However, in the St Paul area, no surface evidence of inversion tectonics exists, nor sub-surface seismic profiles are available, and moreover, pre-rift compression as the main driving mechanism of the folds has been excluded (see Sect. 4.2). Therefore, we consider that the folds formed due to the

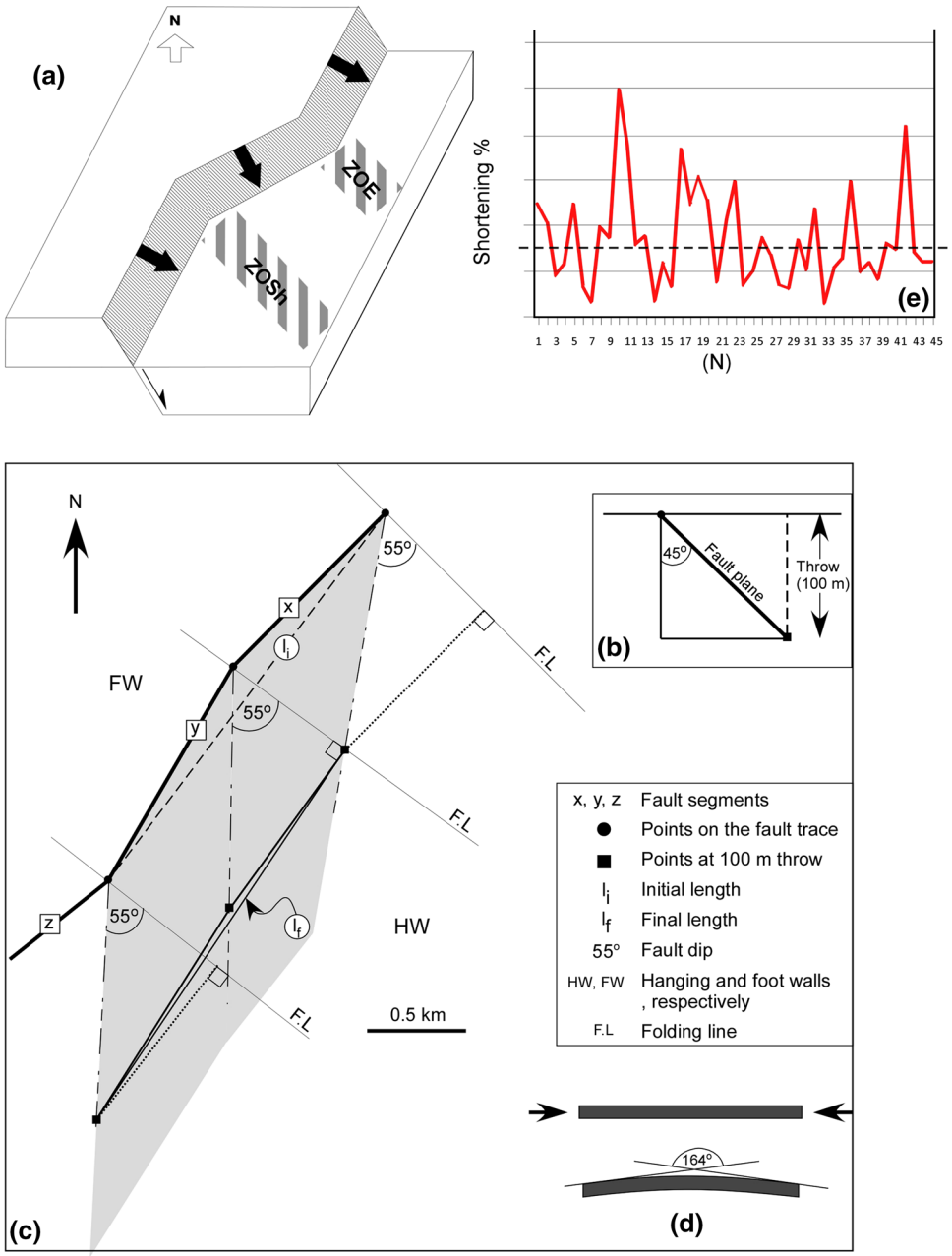

Fig. 13 **a** Development of alternating zones of shortening (ZOSh) and extension (ZOE) due to the movement of the hanging-wall block along the zigzag-shaped fault C. **b** Cross-sectional view of the fault C with a 100 m throw. **c** Total of ~3% shortening, calculated using the orthographic projection technique, caused by the zigzag geometry of the fault C at 100 m throw. d Profile of a very open fold that should have been developed due to the 3% shortening. **e** Amount of shortening calculated by restoring the in- and off-situ deformed ammonites to the undeformed state. The *straight dashed line* is the 3% shortening caused by the zigzag geometry of the fault C

effect of buttressing and to adjust space (Figs. 14c, d, 15). The southeast movement of the less competent, Late Cretaceous, wedge-shaped hanging-wall block of the fault C against the relatively more competent, Eocene, footwall block of the fault B (Figs. 14c, d, 15b, e), which acted as a buttress, would have created a localized zone of NW-SE shortening. The latter shortened the SE-moving block causing it to crumple and fold into meso- to macroscopic scale SSE-plunging folds (Figs. 14d, 15c, f). The amount of shortening along the moving block varies, and is influenced by its wedge geometry. It is greater as the wedge tightens near the northeastern tip and decreases as the wedge widens in the southwest direction. The profile view of the folds along the cross-sectional line X–X′ shows tighter folds having amplitudes of about 80 m, whereas that along cross-sectional line Y–Y′, on the other hand, shows more open folds having amplitude of about 31 m. The amounts of the total shortening along

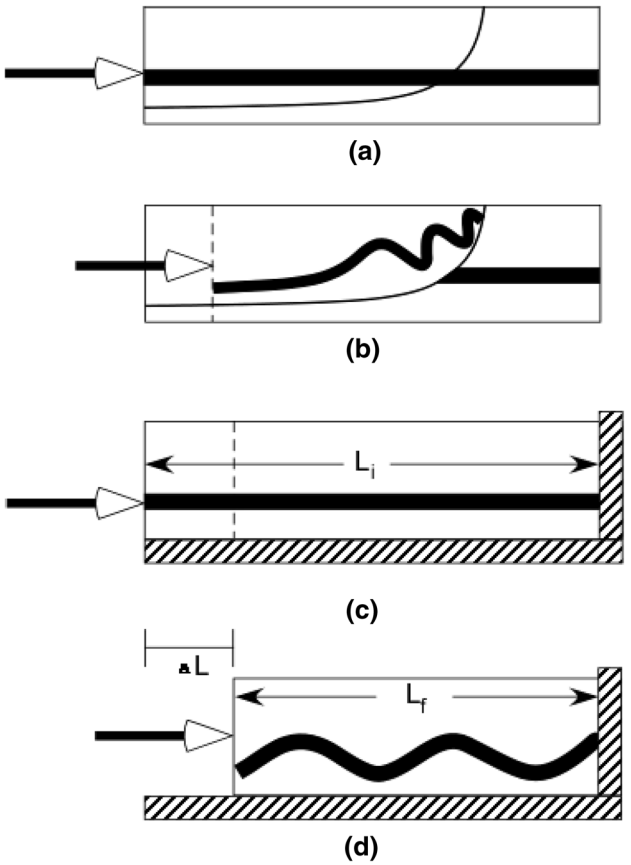

Fig. 14 Schematic diagrams illustrate two models of the development of buttress folds: inverted basin model (**a, b**); and space accommodation problem model (**c, d**). In the latter model, the movement of the solid layer (the hanging wall of fault C in reality) against the vertical stripped stationary edge (fault B in reality) causes the solid layer/hanging-wall block to be shortened and folded

the sections were estimated to be 13.4 and ~9%, respectively (Fig. 3b, c). The wedge-shaped geometry of the moving hanging-wall block together with the heterogeneous deformation explains locally more intense shortening and folding.

The spreading of the plunge direction of the axes of the folded ammonites up to ~40° (from SSE to ESE trending, Fig. 3f) is interpreted to be due to the combination effect of the buttressing, the zigzag geometry of the fault C, and the rotational movement along the minor cross faults that are oriented at high angle to the master NE–SW faults and buttress zones. Given the fact that almost all the deformed ammonites were collected and recorded from very close to the intersection between two segments of the fault C, the zigzag geometry of this fault might have stressed ammonites locally. The minor cross faults may have formed pre, syn, or post the buttress folds (e.g., Dart et al. 1995).

Relative movement along the N–S and NE–SW-trending faults and its significance

Given that the whole area has been extending during rifting, a compelling question arises, what caused the localized shortening between faults B and C? In other words, if both faults were under extension where did the buttressing come from? The answer to this question stems from the fact that in an area under extension, a localized zone of shortening may develop in the shared faulted block between two synthetic faults (Fig. 16). This depends on the slip rate, relative timing, the amount of throw and heave of both faults, and the reactivation of the early-formed fault. Differential amount of throw of the two faults would create the above-mentioned localized zone of shortening provided that the throw of fault C is greater than that of fault B (Fig. 16i). No localized shortening will occur if the early-formed fault is linked to a younger detachment fault. In this case, the detachment fault takes the lead of tectonics, and the early-formed fault acts as a passive fault (Fig. 16ii and iii).

Non-linked faults generally behave independently. Depending on the amount of throw and slip rate of the early-formed outer fault relative to those of the younger one, later reactivation of the former fault results in either extension or shortening of the shared faulted block. The localized shortening will be manifested either by the development of a series of localized folds (Fig. 16iv) or by a reverse fault (Fig. 16v). In all cases, the fault which has the slower slip rate and the smaller throw will act as a buttress to the other fault with the greater throw and faster slip rate (Fig. 16). The amount of shortening increases as the two faults converge downwards due to space accommodation problem.

In the St. Paul case, the amount of throw of fault C was greater than that of fault B. Consequently, the later fault acted as a buttress to the SE-moving hanging-wall block of the fault C.

Body rotation vs. folding of the ammonites

Assuming constant volume homogenous strain, rigid body rotation (or translation) implies zero strain and hence the fossils remain undeformed before and after deformation. The factors that might affect the degree and type of deformation of deformed fossils include: (1) the strain type, whether coaxial or non-coaxial; (2) the fossils dimensions;

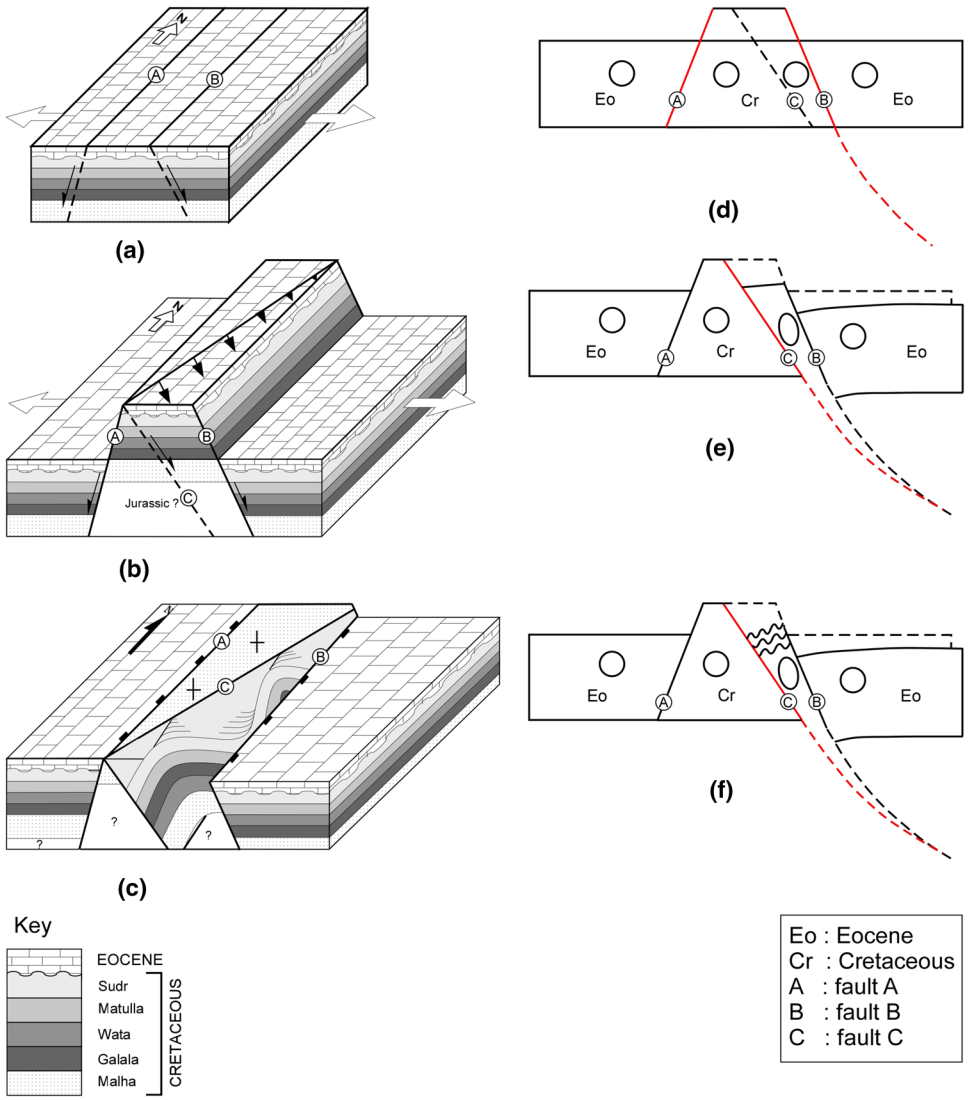

Fig. 15 Schematic 3D (**a**–**c**) and 2D models (**d**–**f**) showing the development of the buttress folds in the St. Paul area during progressive extension. **a** Incipient development of a horst structure between two oppositely dipping N–S-striking normal faults in a horizontally-bedded Cretaceous to Eocene stratigraphic succession. **b, d** Continuous extension intensifies the horst structure due to the pronounced displacement along the faults A and B, and leads to the incipient development of the NE–SW-striking SE-dipping normal fault C in the footwall block of the horst structure. **c, f** Development of buttress folds in the wedge-shaped zone of localized shortening created between the SE-moving hanging-wall block of the fault C and the N–S-striking fault B (see the text for explanation)

(3) the fossils orientations with respect to the applied stresses; (4) the magnitude of the applied differential stresses; (5) matrix bulk strain; and (6) host rock type. The last two factors deal with the competence contrast that is of two main types; layer competence contrast, and fossil-matrix competence contrast. In general, the higher bulk strain the stronger, the deformation of the fossils, and the higher the competence contrast the greater the difference in the finite strain between the fossils/inclusions and the enclosing matrix. However, without strain measurements, it is hard to tell whether a more deformed fossil is due to a higher bulk strain, to a relatively competent matrix, or both. The amount of bulk strain can vary due to the strain partitioning that depends mainly on the fossil-matrix competence contrast, and/or layer competence contrast. Two contrasting scenarios explain the interplay between the deformation partitioning and the competence contrast. In the first scenario, in a stratigraphic succession, the deformation partitions into the less competent or incompetent part of the rock, whether the fossils or the hosting matrix, causing it to be strongly deformed (Fig. 17a–d). Similarly, in an alternating succession of competent-incompetent fossileferous layers, the less or incompetent layers will be strongly deformed than the competent ones, and consequently, the fossils in the latter will be less deformed than in the former. For example, competent fossils embedded in an incompetent or less competent matrix may remain undeformed or slightly deform during ductile deformation (Fig. 17a, b). Similarly, competent fossils will be less deformed than incompetent ones in a common matrix

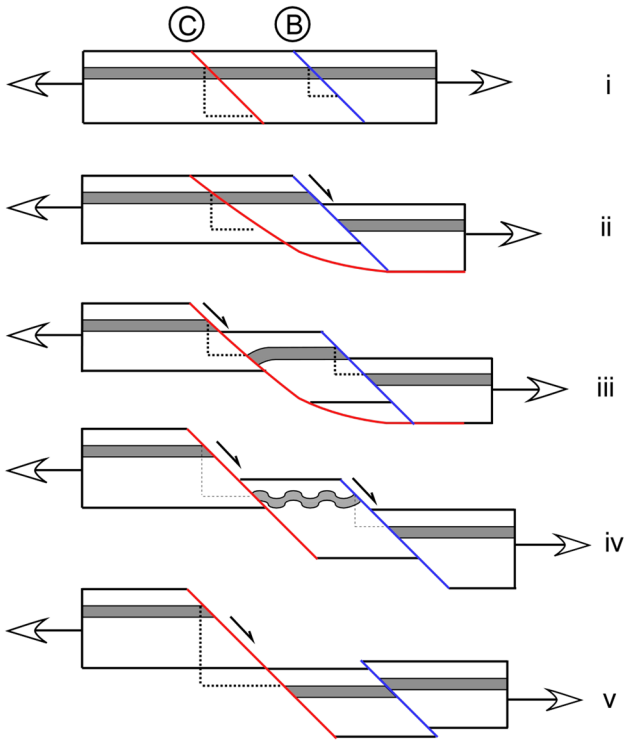

Fig. 16 Schematic diagrams showing the development of a localized zone of shortening due to the differential amount of throw between two rift-related normal faults. **i** Initial development of two faults, B and C with the latter having a greater throw than the former. **ii, iii** Early-formed fault B is linked to the younger detachment fault C. In this case, fault B will passively move along the younger detachment. Movement along the non-linked faults results in a localized zone of shortening manifested either by folding (**iv**) or a reverse fault (**v**)

(Fig. 17e, f). For no or little competence contrast (i.e., the fossils have the same competence as the matrix), the fossils and the matrix deform at the same degree (Fig. 17g, h). In the second scenario, the deformation partitions into the more competent part of the rock, and competent inclusions embedded in an incompetent matrix will be more deformed than the matrix (e.g., Freeman and Lisle 1987). Similarly, in a succession of alternating incompetent-competent layers, a competent layer will be more deformed than incompetent ones during ductile deformation.

In the St. Paul area, the ammonites are embedded in three relatively thin, hard, argillaceous limestone marker beds (Fig. 4a). The folded ammonites occupy the stratigraphically lower two horizons, and are bounded from the bottom by the relatively incompetent calcareous grey shale-dominated Galala Formation (Cenomanian) and from the top by the friable argillaceous sandstone beds of the soft, marl-dominated Wata Formation (Turonian) (Fig. 4a). They are variably sized, some of which attain 50 cm in diameter, lying exactly on the bedding planes, and have the same composition as the enclosing matrix. Consequently, the fossils-matrix competence contrast is negligible or almost zero, whereas the layer competence contrast, i.e., between the ammonite-hosting rock and the upper and lower bounding rocks, is relatively high. Since the extension-related mechanism has been proposed for the formation of the St. Paul folds rather than the simple shear mechanism (i.e., wrench-related folds), a pure shear-like regime was acting during the formation of the St. Paul folds. The horizontal position of the ammonites, almost perpendicular to the localized shortening direction, in one hand, and the regional-scale concentration of deformation in their relatively competent host rocks that is caused by the layer competence contrast, explain why the ammonites appear deformed.

Conclusion

Pre-rift, Late Cretaceous succession in the St. Paul area, the central dip province of the Tertiary Gulf of Suez rift, is folded into a series of extension-related, transverse, gently SSE-plunging folds. The folds are interpreted to be buttress-related structures that are restricted to a wedge-shaped down-faulted block situated between east-and southeast-dipping rift-related normal faults. The relatively incompetent Late Cretaceous hanging-wall block of the southeast-dipping fault moved down-dip past and against a more competent Eocene footwall block of the east-dipping fault. The latter acted as a rigid buttress causing the SE-moving wedge-shaped hanging-wall block to be crumpled and folded. The extension-related buttressing is caused, most probably, by the differential throw of the bounding faults. The combined effect of buttressing, localized stresses caused by the zigzag geometry of the southeast-dipping fault, and the rotational movement along the small scale cross faults probably explain the variable orientations of the axes of the folded ammonites. Unlike the classical buttress folds that form as a consequence of positive basin inversion during compression, the St. Paul buttress-like folds formed in an extensional tectonic setting.

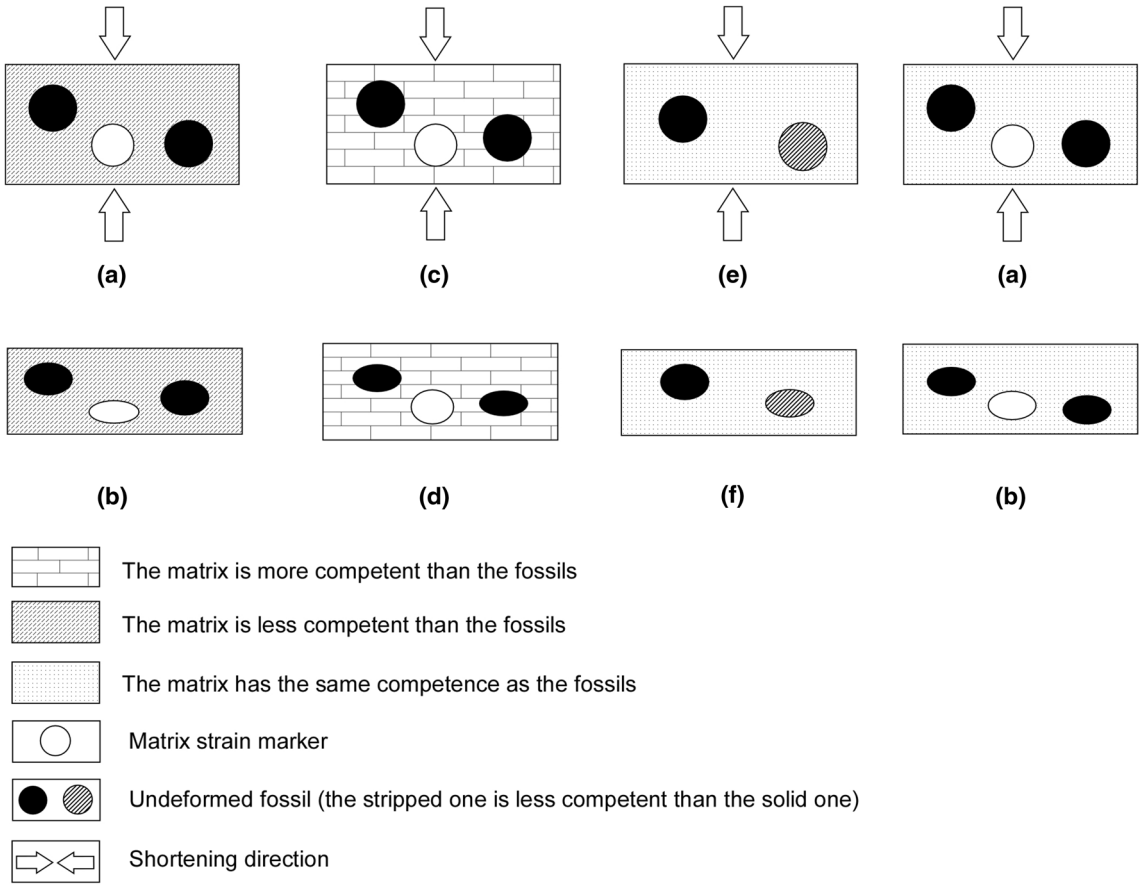

Fig. 17 Diagrams showing the different cases of the fossil-matrix competence contrasts and their effect on the finite strain of both the fossils and the enclosing matrix. **a, b** At high competence contrast (fossils > matrix), the fossils will be less deformed than the surrounding matrix. **c, d** At high competence contrast (fossils < matrix), the fossils will be strongly deformed than the enclosing matrix. **e, f** At high competence contrast with competent and less competent fossils embedded in a matrix, the less competent fossil will be strongly deformed than the competent one. **g, h** At zero competence contrast (fossils = matrix), the fossils and the enclosing matrix deform as the same degree

Acknowledgements The authors would like to thank Beni-Suef University for the facilities provided. The Open Learning Center, Beni-Suef University, is greatly acknowledged for providing the vehicle. Special thanks go to the Suez Oil Company (SUCO), Egypt, for providing a full-board accommodation during the field trip. Prof. Tom Blenkinsop, Cardiff University, UK, is greatly acknowledged for the fruitful discussion and critical comments of the manuscript. Christian Dullo and Monika Dullo are greatly acknowledged for their editorial handling, suggestions, and valuable comments. The driver, Mr. Mahmoud, is acknowledged for the patient and excellent driving.

Appendix

Ammonites

Choffaticeras securiforme (Eck 1909) Early Turonian.

Choffaticeras segne (Solger 1903) Early Turonian.

Coilopoceras requienianum (Orbigny 1841) Late Turonian.

Rubroceras alatum (Cobban et al. 1989) Late Cenomanian.

Thomasites rollandi (Thomas and Peron 1889) Early Turonian.

Thomelites sornayi (Thomel 1966) Late Cenomanian.

Vascoceras cauvini (Chudeau 1909) Late Cenomanian.

Bivalvia

Ceratostreon flabellatum (Goldfuss 1833) Late Cenomanian.

Costagyra olisiponensis (Sharpe 1850) Late Cenomanian.

Eoradiolites liratus (Conrad 1850) Late Cenomanian.

Illymatogyra africana (Lamarck 1801) Late Cenomanian.

Rhynchostreon suborbiculatum (Lamarck 1801) Late Cenomanian.

Echinoids

Hemiaster cubicus (Desor 1847) Late Cenomanian.

References

Abd El-Aziz M, Moustafa AR, Said SE (1998) Impact of basin inversion on hydrocarbon habitat in the Qarun Concession, Western Desert, Egypt. In: Proceedings of 14th EGPC petroleum exploration and production conference Cairo 1, pp 139–155

Abdallah AM, El Adindani A (1963) Notes on the Cenomanian-Turonian contact in the Galala Plateau, Eastern Desert, Egypt. J Geol UAR 7(1):67–70

Abdel-Gawad GI, EL-Qot G, Mekawy MS (2007) Macrobiostratigraphy of the Upper Cretaceous succession from Southern Galala, Eastern Desert, Egypt. In: Youssef E (ed) Proceedings of the 2nd international conference on the geology of tethys, Cairo University, pp 329–349

Abu Khadrah AM, Darwish M, El Azabi MH, Abdel Fattah MA (1987) Lithostratigraphy of Upper Cretaceous-Tertiary succession in the Gulf of Suez (Southern Galala Plateau), Egypt. In: Matheis G, Schandelmeier H (eds) Current research in African earth sciences, pp 171–176. Balkema, Rotterdam

Abu Sharib ASAA (2012) Foliation intersection axes (FIAs) preserved within porphyroblasts: resolving plan view orthogonal refolding, Eastern Fold Belt, Mt Isa Inlier. Aust J Earth Sci 59:571–598

Abu Sharib ASAA (2015) Changes in relative plate motion during the Isan Orogeny(1670–1500 Ma) and implications for Pre-Rodinia Reconstruction. Acta Geol Sin 90(1):88–105

Abu Sharib ASAA, Bell TH (2011) Radical changes in bulk shortening directions during orogenesis: significance for progressive development of regional folds and thrusts. Precambrian Res 188:1–20

Awad GH, Abdallah AM (1966) Upper Cretaceous in Southern Galala, Eastern Desert with emphasis on neighboring areas. J Geol UAR 10 (2):125–144

Bakr A, Helmy M (1990) Wrench faulting and its implication on hydrocarbon accumulations: Alamein-Yidma area, Western Desert, Egypt. In: Proceedings of 10th EGPC petroleum exploration and production conference vol 2, pp 257–289

Baum MS, Withjack MO, Schlische RW (2008) The ins and outs of buttress folds: examples from the inverted fundy rift basin, Nova Scotia and New Brunswick, Canada. Reprinted from Conjugate Margins Conference, Halifax

Beck WC, Chapin CE (1994) Structural and tectonic evolution of the Joyita Hills, central New Mexico: implications of basement control on Rio Grande rift. In: Keller GR, Cather SM (eds) Basins of the Rio Grande rift: structure, stratigraphy and tectonic setting: Geological Society of America Special Paper 291, 187–205

Bederke E (1966) The development of European rifts. In: Irvin TN (ed) The world rift system: Geological Survey of Canada Paper 66–14 pp 213–219

Bosworth W (1995) A high-strain rift model for the southern Gulf of Suez (Egypt). Geol Soc Lond Special Publ 80:75–102

Bosworth W, McClay KR (2001) Structural and stratigraphic evolution of the Gulf of Suez rift, Egypt: a synthesis. In: Zeigler PA, Cavazza W, Robertson AHFR, Crasquin-Soleau S (eds) Peri-Tethys Memoir 6: 'Peritethyan Rift/Wrench Basins and Passive Margins'. Memoires du Museum National d'Historie Naturelle de Paris vol 186, pp 567–606

Boyer SE, Eliott D (1982) Thrust systems. Am Assoc Petr Geol 66(9):1196–1230

Coffield DQ, Schamel S (1989) Surface expression of an accommodation zone within the Gulf of Suez rift, Egypt. Geology 17(1):76

Colletta B, Le Quellece P, Letouz J, Moretti I (1988) Longitudinal evolution of the Suez rift structures (Egypt). Tectonophysics 153:221–233

Corfield S, Sharp IR (2000) Structural style and stratigraphic architecture of fault propagation folding in extensional settings. A seismic example from the Smørbukk area. Basin Research, Halten Terrace, mid-Norway

Dart CJ, McClay K, Hollings PN (1995) 3D analysis of inverted extensional fault systems, southern Bristol Channel basin, UK. Geological Society, London, Special Publications 88(1):393–413

Davis GH, Reynolds SJ, Kluth CF (2012) Structural geology of rocks and regions, 3rd edn. Wiley, Amsterdam, p 864

El-Shaarawy OA, Abdel Aal A, Papazis P (1992) Tectonic setting of the Razzak oil field, north Western Desert of Egypt. In: Proceedings of the 11th EGPC Exploration and Production Conference (Cairo) 2:310–323

Faulds JE, Geissman JW, Mawer CK (1990) Structural development of major extensional accommodation zone in the Basin and Range province, northwestern Arizona and southern Nevada: implication for kinematic models of continental extension. In: Wernicke BP (ed) Basin and Range extensional tectonics near the latitude of Las Vegas. Geological Society of America Memoir, Nevada, pp 37–76

Faulds JE, Olson EL, Harlan SS, McIntosh WC (2002) Miocene extension and fault-related folding in Highland Range, southern Nevada: a three-dimensional perspective. J Struct Geol 24:861–886

Florensov NA (1966) The Baikal rift zone. In Irvin TN (ed) The world rift system: Geological Survey of Canada Paper, 66–14 pp 173–180

Freeman B, Lisle RJ (1987) The relationship between tectonic strain and the three-dimensional shape fabrics of pebbles in deformed conglomerates. J Geol Soc 144(4):635–639

Galal G, Kamel S (2007) Early Paleogene planktonic foraminiferal biostratigraphy at the Monastery of Saint Paul, Southern Galala, Eastern Desert, Egypt. In: Bice K et al. (eds) Revue de Paléobiologie, Genève, 26 (2): 391–402

Garfunkel Z, Bartov Y (1977) The tectonic of the Suez rift. Geol Surv Israel Bull 71:1–44

Gawthorpe RL, Sharp I, Underhill JR, Gupta S (1997) Linked sequence stratigraphic and structural evolution of propagating normal faults. Geology 25:795–798

Gupta SH, Underhill JR, Sharp I, Gawthorpe RL (1999) Role of fault interaction in controlling syn-rift dispersal pattern: Miocene, Abu Alaqa Group, Suez Rift, Sinai, Egypt. Basin Res 11:167–189

Höntzsch S, Scheibner C, Kuss J, Marzouk AM, Rasser MW (2011) Tectonically driven carbonate ramp evolution at the southern Tethyan shelf: the Lower Eocene succession of the Galala Mountains, Egypt. Facies 57:51–72

Janecke SU, Vandenburg CJ, Blankenau JJ (1998) Geometry, mechanism and significance of extensional folds from examples in the Rocky Mountain Basin and Range Province, USA. J Struct Geol 20:841–856

Jarrige J, Ott d'Estevou P, Burollet PF, Thiriet JP, Icart JC, Richert JP, Sehans P, Montenat C, Prat P (1986) Inherited discontinuities and neogene structure: the Gulf of Suez and the Northwestern edge of the Red sea. Philos Trans R Soc Lond 317:129–139

Jarrige J-J, Ott d'Estevou P, Burollet PF, Montenat C, Prat P, Richert J-P, Thiriet J-P (1990) The multistage tectonic evolution of

the Gulf of Suez and northern Red Sea continental rift from field observations. Tectonics 9(3):441–465
Kazmin V (1979) Relationship between rifts and Precambrian basement in East Africa. Ann Geol Surv Egypt 9:54–60
Khalil SM, McClay KR (2002) Extensional fault-related folding, northwestern Red Sea, Egypt. J Struct Geol 24(4):743–762
Kuss J, Scheibner C, Gietl R (2000) Carbonate platform to basin transition along an Upper Cretaceous to Lower Tertiary Syrian arc uplift, Galala Plateau, Eastern Desert, Egypt. Geol Arabia 5: 405–424
Lyberis N (1988) Tectonic evolution of the Gulf of Suez and the Gulf of Aqaba. Tectonophysics 153(1-4):209–220
Maurin J-C, Niviere B (1999) Extensional forced folding and decollement of the pre-rift series along the Rhine graben. In: Cosgrove JW, Ameen MS (eds) Forced folds and fractures, Special Publication vol 169, pp 73–86
McClay KR, Nicols GJ, Khalil SM, Darwish M, Bosworth W (1998) Extensional tectonics and sedimentation, Eastern Gulf of Suez, Egypt. In: Purser BH, Bosence DWJ (eds) Sedimentation and tectonics of Rift Basins, Red Sea-Gulf of Aden. Chapman and Hall, London, pp 223–238
McConell RB (1972) Geological developments of the rift system in eastern Africa. Geol Soc Am Bull 100:1361–1374
Meshref WM (1990) Tectonic framework. In: Said R (ed) The Geology of Egypt. A.A. Balkema-Rotterdam-Bookfield, pp 113–155
Misra AA, Mukherjee S (2015) Tectonic inheritance in continental rifts and passive margins. Spring Brief Earth Sci
Moretti I, Chénet PY (1987) The evolution of the Suez rift: a combination of stretching and secondary convection. Tectonophysics 133(3-4):229–234
Morley CK, Nelson RA, Patton TL, Munn SG (1990) Transfer zones in the East African Rift system and their relevance to hydrocarbon exploration in rifts. Am Assoc Pet Geol Bull 74:1234–1253
Moustafa AR (1987) Drape folding in the Baba-Sidri area, Eastern side of the Suez rift, Egypt. Egypt J Geol 31:15–27
Moustafa AR (1993) Structural characteristics and tectonic evolution of the east margin blocks of the Suez rift. Tectonophysics 223:381–399
Moustafa AR (2002) Controls on the geometry of transfer zones in the Suez Rift and Northwest Red Sea: implications for the structural geometry of Rift Systems. AAPG Bull 86:979–1002
Moustafa AR (2008) Mesozoice–Cenozoic basin evolution in the northern Western Desert of Egypt. In: Salem M, El-Arnauti A, Saleh A (eds) 3rd Symposium on the Sedimentary Basins of Libya, The Geology of East Libya, 3:29–46
Moustafa AR (2013) Fold-related faults in the Syrian Arc belt of northern Egypt. Mar Petrol Geol 48:441–454
Moustafa AR, El-Raey AK (1993) Structural characteristics of the Suez rift margins. Geol Rundsch 82:101–109
Moustafa AR, Khalil MH (1995) Superposed deformation in the northern Suez rift, Egypt: relevance to hydrocarbon exploration. J Petrol Geol 18:245–266
Moustafa AR, El-Barkooky AN, Mahmoud A, Badran AM, Helal MA, Nour El Din M, Fathy H (2002) Matruh basin: hydrocarbon plays in an inverted Jurassice–Cretaceous rift basin in the northern Western Desert of Egypt (abs). In: AAPG international meeting (Cairo)
Moustafa AR, Abd El-Aziz M, Gaber W (2008) Tiba – Natrun – Kattaniya basin, northern Western Desert (Egypt): impact of fault orientations on basin inversion. In: Salem MJ, El-Hawat AS (eds) 3rd Symposium on the sedimentary Basins of Libya, The Geology of East Libya, 1: 295–310
Mukherjee S (2011) Flanking Microstructures from the Zanskar Shear Zone, NW Indian Himalaya. YES Bull 1:21–29
Mukherjee S (2014) Review of flanking structures in meso- and micro-scales. Geol Magn 151:957–974
Mukherjee S, Koyi HA (2009) Flanking microstructures. Geol Magn 146:517–526
Nemec MC (1996) Qarun oil field, Western Desert, Egypt. In: Proceedings of 13th EGPC petroleum conference pp 140–164
Oesterlen P, Blenkinsop T (1994) Extension directions and strain near the failed triple junction of the Zambezi and Luangwa Rift zones, southern Africa. J Afr Earth Sci 18:175–180
Patton TL (1982) Surface studies of normal fault geometries in the pre-Miocene stratigraphy, west central Sinai Peninsula. In: Proceedings of the 6th Egyptian general petroleum corporation exploration Seminar, Cairo vol 1, pp 437–452
Patton TL, Moustafa AR, Nelson RA, Abdine SA (1994) Tectonic evolution and structural setting of the Suez Rift. In: Landon SM (ed) Interior Rift Basins. AAPG Memoir 59:7–55
Purser BH, Bosence DWJ (eds) (1998) Sedimentation and Tectonics of Rift Basins: Red Sea-Gulf of Aden. Chapman and Hall, London, p 663
Rosendahl BR (1987) Architecture of African rifts with special reference to East Africa. Ann Rev Earth Planet Sci 15:455–503
Scheibner C, Marzouk AM, Kuss J (2001) Maastrichtian-Early Eocene litho- biostratigraphy and palaeogeography of the northern Gulf of Suez region, Egypt. J Afr Earth Sci 32:223–255
Schilsche RW (1992) Anatomy and evolution of Triassic-Jurassic continental rift system, Eastern North America. Tectonics 12:1026–1042
Schilsche RW (1995) Geometry and origin of fault-related folds in extensional settings. Am Assoc Petrol Geol Bull 79:1661–1678
Schutz KI (1994) Structure and stratigraphy of the Gulf of Suez, Egypt. In: Landon SM (ed) Interior Rift Basins AAPG Mem vol 59, pp 57–96
Sehim A, Frisch W, Noufal A (1999) Paleostress status and rifting events of the Gulf of Suez basin, Egypt. In: Hafez AM (ed) Proceedings of the 4th International Conference of the Geology of Arab World, Cairo, Egypt vol 2, pp 46–79
Sharp I, Gawthorpe RL, Underhill JR, Gupta S (2000) Fault propagation fold in extensional settings: example of structural style and syn-rift sedimentary response from the Suez Rift, Sinai, Egypt. Bull Geol Soc Am 112:1877–1899
Twiss RJ, Moores EM (2007) Structural geology. W. H. Freeman and Company, New York (2nd edition), p 736
Vargo JM, Greer MJ, Collins BP, Davies CB, Miller Jr MH (1993) Gulf of Suez plays center on tilted fault blocks. World Oil 5:60–74
Younes AI, McClay K (1998) Role of basement fabric on Miocene rifting in the Gulf of Suez-Red Sea: In: Proceedings of the 14th Egyptian general petroleum corporation, petroleum conference, vol 1, pp 35–50
Younes A, McClay K (2002) Development of accommodation zones in the Gulf of Suez-Red Sea rift, Egypt. AAPG Bull 86:1003–1026